Behavioral/Systems/Cognitive

Expression of Connexin36 in Cone Pedicles and OFF-Cone Bipolar Cells of the Mouse Retina

Andreas Feigenspan,[1] Ulrike Janssen-Bienhold,[1] Sheriar Hormuzdi,[2] Hannah Monyer,[2] Joachim Degen,[3] Goran Söhl,[3] Klaus Willecke,[3] Josef Ammermüller,[1] and Reto Weiler[1]

[1]Institute of Biology, University of Oldenburg, D-26111 Oldenburg, Germany, [2]Department of Clinical Neurobiology, University Hospital of Neurology, D-69120 Heidelberg, Germany, and [3]Institute for Molecular Genetics, University of Bonn, D-53117 Bonn, Germany

Transgenic technology, immunocytochemistry, electrophysiology, intracellular injection techniques, and reverse transcription PCR were combined to study the expression of neuronal connexin36 (Cx36) in the outer plexiform layer of the mouse retina. Transgenic animals expressed either a fusion protein of full-length Cx36 with enhanced green fluorescent protein (EGFP) attached at the C terminus or exon 2 of Cx36 was replaced by β-galactosidase (β-gal). In the outer nuclear layer, β-gal-positive cell bodies, which were confined to the most distal region close to the outer limiting membrane, displayed immunoreactivity against S-cone opsin. Cx36 –EGFP puncta colocalized with cone pedicles, which were visualized by intracellular injection. In reverse transcriptase PCR experiments, Cx36 mRNA was never detected in samples of rods harvested from the outer nuclear layer. These results strongly suggest expression of Cx36 in cones but not in rods. In vertical sections, Cx36 expression in the vitreal part of the outer plexiform layer was characterized by a patchy distribution. Immunocytochemistry with antibodies against the neurokinin-3 receptor and the potassium channel HCN4 (hyperpolarization-activated cyclic nucleotide-gated potassium channel) displayed clusters of the Cx36 label on the dendrites of OFF-cone bipolar cells. In horizontal sections, these clusters of Cx36 appeared as round or oval-shaped groups of individual puncta, and they were always aligned with the base of cone pedicles. Double-labeling experiments and single-cell reverse transcriptase PCR ruled out expression of Cx36 in horizontal cells and rod bipolar cells. At light microscopic resolution, we found close association of Cx36 –EGFP with the AMPA-type glutamate receptor subunit GluR1 but not with GluR2–GluR4, the kainate receptor subunit GluR5, or the metabotropic glutamate receptor mGluR6.

Key words: **gap junctions; connexin; retina; rods; cones; bipolar cells; glutamate receptors**

Introduction

Gap junctions are intercellular connections between adjacent cells and thus provide the structural basis for metabolic and electrical coupling. Gap junction channels are encoded by the connexin (Cx) family of genes, with at least 19 and 20 members in the murine and human genome, respectively (Eiberger et al., 2001; Willecke et al., 2002). Six connexin proteins associate to form a connexon or hemichannel, and the docking of two hemichannels located in opposing membranes leads to the generation of a functional gap junction between the cells. Connexons can be assembled from the same (homomeric) or from different (heteromeric) types of connexin proteins, which impart variability in their biophysical properties and potential intracellular regulatory sites.

Connexin-based channels are permeable to metabolites with a molecular mass of up to 1 kDa as well as to inorganic ions, forming a low-resistance pathway to current flow between cells. In the adult brain, gap junctions mediate temporal coordination of neuronal activity (Strata et al., 1997; Mann-Metzer and Yarom, 1999), and they are responsible for synchronized spiking of inhibitory cortical interneurons (Benardo, 1997; Galarreta and Hestrin, 1999; Gibson et al., 1999; Tamas et al., 2000; Venance et al., 2000) and high-frequency oscillations (Draguhn et al., 1998; Traub et al., 1999). Although mRNAs for several Cx genes have been detected in the rodent brain, the molecular identities of most neuronal connexins remain unresolved. Only Cx36 has been unequivocally identified at neuronal gap junctions in an ultrastructural study (Rash et al., 2000). Expression of Cx36 has been demonstrated in various parts of the brain and the retina (Condorelli et al., 2000; Güldenagel et al., 2000; Rash et al., 2000; Feigenspan et al., 2001; Meier et al., 2002; De Zeeuw et al., 2003). In the neocortex and the hippocampus, Cx36 is expressed by interneurons and has proved critical for the generation of synchronous inhibitory activity (Venance et al., 2000; Deans et al., 2001). Loss of Cx36-containing gap junctions in Cx36-deficient mice disrupts γ-frequency network oscillations in the hippocampus (Hormuzdi et al., 2001).

In the rodent retina, Cx36 has been localized to AII amacrine cells (Feigenspan et al., 2001; Mills et al., 2001). Because AII amacrine cells are central elements of the primary rod pathway, disruption of Cx36 leads to impairment of visual signal transmission under scotopic conditions (Güldenagel et al., 2001). Besides being expressed in AII amacrine cell dendrites in the inner plex-

Received Sept. 26, 2003; revised Jan. 22, 2004; accepted Jan. 23, 2004.

This work was supported by the Deutsche Forschungsgemeinschaft (Sonderforschungsbereich 517, Wi270/22-3/4) and the Fonds of the Chemical Industry. We thank Jennifer Shelley for reading and improving this manuscript and Susanne Wallenstein for excellent technical assistance.

Correspondence should be addressed to Dr. Andreas Feigenspan, Institute of Biology, University of Oldenburg, D-26111 Oldenburg, Germany. E-mail: andreas.feigenspan@uni-oldenburg.de.

DOI:10.1523/JNEUROSCI.5598-03.2004

 0270-6474/04/243325-10$15.00/0

Table 1. Sources and working dilutions of antibodies

Antigen	Antiserum	Source	Working dilution
GluR1	Rabbit anti-GluR1	Pharmingen, Heidelberg, Germany	1:100–1:200
GluR5 (N-19)	Goat anti-GluR5	Santa Cruz Biotechnology, Santa Cruz, CA	1:100
mGluR6	Rabbit anti-mGluR6	Acris, Neuromics, Hiddenhausen, Germany	1:500
S-cone opsin	Rabbit anti-S-cone opsin	Dr. J. Nathans, Johns Hopkins University, Baltimore, MD	1:5000
PKC	Mouse anti-PKC, clone MC5	Pharmingen	1:200
Caldendrin	Guinea pig anti-caldendrin	Dr. E. D. Gundelfinger, Magdeburg, Germany	1:2000
HCN4	Rabbit anti-HCN4	Alomone, Jerusalem, Israel	1:500
NK3R	Rabbit anti-NK3R	Acris; Novus Biologicals, Littleton, CO	1:250–1:500
Bassoon	Mouse anti-bassoon, clone VAM-PS003	StressGen, San Diego, CA	1:500
Synaptophysin	Mouse anti-synaptophysin, clone SVP-38	Sigma	1:200
Cx36	Rabbit anti-Cx36	Zytomed, Berlin, Germany	1:200
Calbindin	Rabbit anti-calbindin	Swant, Bellinzona, Switzerland	1:500

iform layer (IPL) of the rodent retina, Cx36 immunoreactivity is also present in the outer plexiform layer (OPL). The physiological significance of Cx36-containing gap junctions in multiple rod pathways has been proposed recently by a study using transgenic mice in which the Cx36 coding sequence was replaced with histological markers (Deans et al., 2002). We used two transgenic mouse lines to investigate the cellular origin of Cx36 expression in the OPL. In contrast to the results of Deans et al. (2002), we found expression of Cx36 in cones but not in rods. In addition, Cx36 is accumulated in patches on dendrites of OFF-cone bipolar cells, displaying colocalization with the glutamate receptor subunit GluR1.

Materials and Methods

Tissue preparation. Mice carrying a targeted replacement of Cx36 exon 2 by β-galactosidase (β-gal) cDNA ($Cx36^{LacZ}$ strain) were established by ubiquitous deletion of a floxed Cx36 allele, generated by J. Degen (unpublished results), using a strategy similar to that used to generate $Cx43^{del}$ animals (Theis et al., 2001). Adult transgenic $Cx36^{Cx36-EGFP}$ mice and $Cx36^{LacZ/LacZ}$ mice were deeply anesthetized by intraperitoneal injection of a 0.1 ml solution containing equal parts of 5% ketamine (Ceva, Düsseldorf, Germany) and 1% xylazine (Ceva) and subsequently killed by cervical dislocation. After removal of cornea, lens, and vitreous body, the eyecup with the retina still attached was fixed in 2% paraformaldehyde (PA) in 0.1 M phosphate buffer (PB), pH 7.4, for 20 min. After fixation, the tissue was cryoprotected in 30% sucrose, embedded in 10% gelatin, and sectioned vertically or horizontally at 12 μm thickness with a cryostat. Sections were either processed immediately or stored at −20°C no longer than 4 weeks.

For the preparation of slices, the retina of $Cx36^{Cx36-EGFP}$ mice was removed from the eyecup and embedded in 2% agarose in Ames medium (Sigma, Deisenhofen, Germany). Agar blocks were mounted on a vibratome (Leica, Nussloch, Germany) and cut into slices of 200 μm thickness. The slices were immediately fixed in 2% PA for 3–5 min, washed in Tyrode's solution, and subsequently transferred to the stage of an upright microscope (Leica) for intracellular injections.

Immunocytochemistry, histochemistry, and intracellular injections. Sources and working dilutions of antibodies are listed in Table 1. For immunocytochemistry, cryosections were incubated in a solution containing 5% normal goat serum (NGS) and 0.3% Triton X-100 in PB for 1 hr. Primary antibodies were diluted in 3% NGS and 0.3% Triton X-100 in PB and applied overnight at 4°C. After washes in PB, secondary antibodies, dissolved in 1% NGS and 0.3% Triton X-100 in PB, were applied for 2 hr at room temperature. Secondary antibodies were conjugated to Alexa Fluor 488, Alexa Fluor 568 (Molecular Probes, Eugene, OR), Cy3, or Cy5 (Dianova, Hamburg, Germany). In double-labeling experiments, sections were incubated in a mixture of primary antibodies, followed by a mixture of secondary antibodies.

β-gal histochemical analysis was performed on cryosections from $Cx36^{LacZ/LacZ}$ mice. Basic buffer contained the following (in mM): 100 sodium phosphate buffer, pH 7.4, 2 $MgCl_2$, and 5 EGTA, pH 8.0. Wash buffer contained 0.01% sodium deoxycholate and 0.02% NP-40 (Amersham Biosciences, Piscataway, NJ) dissolved in basic buffer. Stain buffer contained 5 mM potassium ferrocyanide, 5 mM potassium ferricyanide, and 1 mg/ml 5-bromo-4-chloro-3-indolyl-β-D-galactopyranoside (X-gal) (Amersham Biosciences) dissolved in wash buffer. X-gal was prepared as 25 mg/ml stock solution in dimethylformamide and stored at −20°C. Sections were incubated in stain buffer for 8–24 hr at 37°C in the dark. Immunocytochemistry was performed after β-gal histochemistry. With the exception of antibodies against the neurokinin-3 receptor NK3R, the histochemical procedure for LacZ did not interfere with subsequent binding of primary antibodies.

Intracellular injections were performed with sharp borosilicate microelectrodes (Hilgenberg, Malsfeld, Germany) filled with 10 mM Alexa Fluor 594 hydrazide (Molecular Probes). Alexa 594 was injected iontophoretically (5–10 min, −1 nA) into the somata of morphologically identified cells using the current-clamp circuit of the EPC-9 patch-clamp amplifier (Heka, Lambrecht, Germany). After injection, slices were postfixed in 2% PA for 30 min, washed in PB, and processed for immunocytochemistry as described above.

Sections processed for β-galactosidase were viewed using a Zeiss (Oberkochen, Germany) axiophot microscope, and images were taken with an AxioCam MRC digital camera (Zeiss). Confocal micrographs of fluorescent specimens were taken with a Leica TCS SL confocal microscope equipped with an argon and a helium–neon laser. Scanning was performed with a 40×/1.25 Plan-Apochromat and a 63×/1.32 Plan-Apochromat objective at a resolution of 1024 × 1024 pixels. Different wavelength scans were performed sequentially to rule out cross talk between red, green, and blue channels. Images were superimposed and adjusted in brightness and contrast using Photoshop 5.5 (Adobe Systems, San Jose, CA).

Statistical analysis of colocalization of confocal images. Pedicles of dye-injected cones were tiled with 32 × 32 pixel squares. Enhanced green fluorescent protein (EGFP) puncta located on the pedicles were centered in the middle of a square. All squares were clipped from the image, converted into a matrix of appropriate dimensions, and subsequently averaged using Microcal Origin software (Microcal Software, Northampton, MA). The averaged matrix was plotted using the matrix values, i.e., the brightness of each pixel, as information in the z-dimension. Control images were obtained by projecting a mirror image of the EGFP pattern onto the cone pedicle and performing the same calculations as above. In general, squares fully covered by the pedicle do not contribute to the peaked distribution but instead decrease signal-to-noise ratio and thus the height of the center peak.

Detection of rhodopsin and Cx36 transcripts in photoreceptors using reverse transcription-PCR. RNA was extracted from mouse retina by means of an RNA preparation kit (NucleoSpin RNAII; Macherey-Nagel, Düren, Germany) according to the protocol of the manufacturer. To obtain photoreceptor mRNA, the isolated mouse retina was sectioned into slices of 200 μm thickness on a vibratome (Leica). Individual slices were placed

in a recording chamber and superfused with Tyrode's solution. Ten to 20 photoreceptor cell bodies were harvested from appropriate regions of the outer nuclear layer (ONL) using a patch pipette. The pipette was filled with a solution containing 130 mM KCl, and photoreceptors were aspirated into the pipette tip by applying negative pressure. Subsequently, the tip of the pipette was broken into a PCR tube containing 20 U of RNase inhibitor (Rnasin; Promega, Madison, WI), and the sample (~8 μl) was subjected to a brief centrifugation. Contaminating genomic DNA was digested with DNase I (Amplification Grade; Invitrogen, Carlsbad, CA) according to the protocol of the manufacturer. cDNA synthesis from 2–4 μg of retinal RNA and from the photoreceptor samples was performed in final volumes of 50 and 25 μl, respectively. The samples contained 1× first-strand buffer (Promega), 0.6 μM oligo-dT primer (Promega), 0.6 μM random primer (Promega), 0.5 mM of each dNTP (Eppendorf, Hamburg, Germany), and 0.8 U/μl RNasin RNase inhibitor (Promega). After primer annealing for 10 min at 72°C, the samples were briefly chilled on ice and incubated for 2 min at 42°C, before 0.3 U/μl avian myeloblastosis virus reverse transcriptase (Promega) were added. cDNA synthesis was performed for 1 hr at 42°C and stopped by incubating the samples for 5 min at 95°C. cDNA was stored at −20°C.

PCR reactions were performed in a total volume of 25 μl. This included 2 and 6 μl retinal and photoreceptor cDNA, respectively, 1× reaction buffer (Promega), 1.25 mM $MgCl_2$, 0.2 mM of each dNTP (Eppendorf), 0.8 μM of each primer (MWG Biotech, Ebersberg, Germany), and 1 U of *Taq* polymerase (Promega). Reactions were overlaid with 35 μl of mineral oil (Sigma). The *Taq* polymerase was added after incubating the samples for 2 min at 95°C (hot start). The specific primer set for the detection of rhodopsin included the sense primer (5′-CATTGAGCGCTAC GTGGTGGTC-3′) and the antisense primer (5′-ATGAAGATGGGGCCGAAGTTGG-3′), both of which were designed according to the mouse rhodopsin coding sequence (GenBank accession number RNY16898; the predicted size of the amplicon was 766 bp). Cx36 expression was analyzed by two different sets of specific primers, designed according to the coding sequence of mouse Cx36 (GenBank accession number AF016190). One intron-spanning primer set revealed an amplicon with a predicted size of 766 bp (sense, 5′-GCAGCAGCACTCCACTATGATTG-3′; antisense, 5′-CAGCCAGATTGAGCACCACAC-3′) and the other of 447 bp (sense, 5′-TGCAGCAGCACTCCACTATGA TTG-3′; antisense, 5′-GTCTCCTTACTGGTGGTCTCTGTG-3′). Amplifications of rhodopsin and Cx36 transcripts were performed under the same conditions in a Stratagene (La Jolla, CA) Robocycler and at the same time (40 cycles of 95°C for 0.5 min, 58°C for 1 min, 72°C for 2 min, and a final extension at 72°C for 15 min). Twenty microliters of each amplification product were analyzed on a 2% agarose gel and visualized on a transilluminator after ethidium bromide staining.

Electroretinogram measurements. Animals were dark-adapted overnight before commencement of recordings. Mice were anesthetized by intraperitoneal injections of xylazine (50 mg/kg) and ketamine (20 mg/kg), and the pupils were dilated with 1% atropine sulfate. Surgery and subsequent handling were done under dim red dark-room light. A continuously moistened Ag/AgCl cotton-wick electrode was placed on the corneal surface, and a platinum reference electrode was inserted subcutaneously into the skin covering the skull. A platinum ground electrode was inserted into the tail. The mouse was placed sideways with the head fixed. Electrical potentials were recorded and bandpass filtered (1 Hz to 1000 Hz) using a DAM50 Bioamplifier (World Precision Instruments, Sarasota, FL). Online averaging and storage were performed with the MacLab system (AD Instruments, Hastings, UK) connected to an Apple Computers (Cupertino, CA) PowerPC. Full-field test lights were generated with a 150 W halogen light source and focused onto the cornea. Intensities were adjusted with neutral-density filters. Test flash duration was 20 msec. Corneal illuminance for white light (in lux) was measured with a calibrated luxmeter (Palux; Gossen, Nürnberg, Germany) at the position of the cornea.

Scotopic intensity–response curves were measured with a stimulus interval of 10 sec. Ten responses were averaged for each intensity. For analysis, overall response amplitudes were measured relative to the baseline, which was determined by the mean voltage within a 30 msec period before the light flash. Oscillatory potentials were included in the overall amplitude. Implicit time was determined as the temporal difference between light onset and the time at which maximum response was reached.

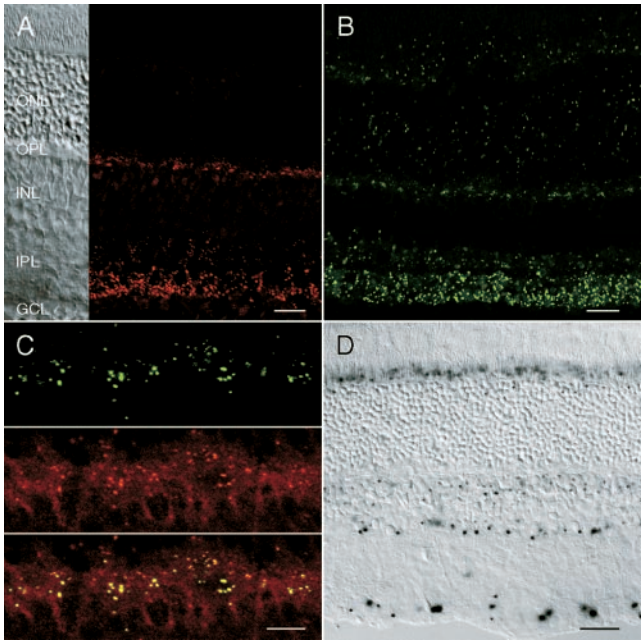

Figure 1. Expression of Cx36 in wild-type and transgenic mouse retina. *A*, Immunolabeling of vertical sections of wild-type mouse retina with polyclonal antibodies to Cx36. *B*, Expression pattern of EGFP in $Cx36^{Cx36-EGFP}$ transgenic mice. *C*, High-power confocal micrograph showing the OPL of $Cx36^{Cx36-EGFP}$ mice counterstained with Cx36 antibodies. Top, EGFP staining pattern; middle, Cx36 immunoreactivity; bottom, superimposition of EGFP and Cx36 immunolabeling. Yellow indicates overlap of EGFP and Cx36 immunofluorescence. *D*, Expression pattern of β-galactosidase in $Cx36^{LacZ/LacZ}$ transgenic mice. Scale bars: *A*, *B*, *D*, 20 μm; *C*, 10 μm. Nomarski image in *A* indicates layering of the mouse retina. GCL, Ganglion cell layer.

Results

Transgenic animal models

Polyclonal antibodies directed to the C-terminal region of human Cx36 label both plexiform layers in a vertical section of the mouse retina (Fig. 1*A*). Whereas expression of Cx36 in AII amacrine cells causes punctate immunoreactivity in the inner plexiform layer (Feigenspan et al., 2001; Mills et al., 2001), the cellular origin of the label in the outer plexiform layer is currently under debate. Unfortunately, the antibodies to Cx36 are not ideally suited to study this question, because they require a different fixation protocol than other antibodies used in this study, thus making most double labelings impossible.

To identify the cell types containing Cx36 in the outer mammalian retina, we used two different transgenic mouse lines. The first line, $Cx36^{Cx36-EGFP}$, expresses a fusion protein of Cx36 and EGFP, with EGFP being attached to the C terminal of Cx36. Using standard immunocytochemical markers, we detected no changes in the morphology of $Cx36^{Cx36-EGFP}$ mouse retinas with regard to cell types and numbers of cells. The distribution of EGFP in both plexiform layers closely resembles the staining pattern obtained with the polyclonal antibodies (Fig. 1*B*). In fact, both EGFP and antibody labeling performed in the same vertical section of $Cx36^{Cx36-EGFP}$ mice correspond almost perfectly, as shown for the OPL (Fig. 1*C*). The same holds true for the IPL (data not shown), indicating precise targeting of the chimeric protein to homologous and heterologous gap junctions in both synaptic layers. In the outer retina, EGFP puncta appear as clusters in the vitreal part of the OPL but are rather diffusely distributed in the scleral part (Fig. 1*B*,*C*). Finally, the entire ONL and

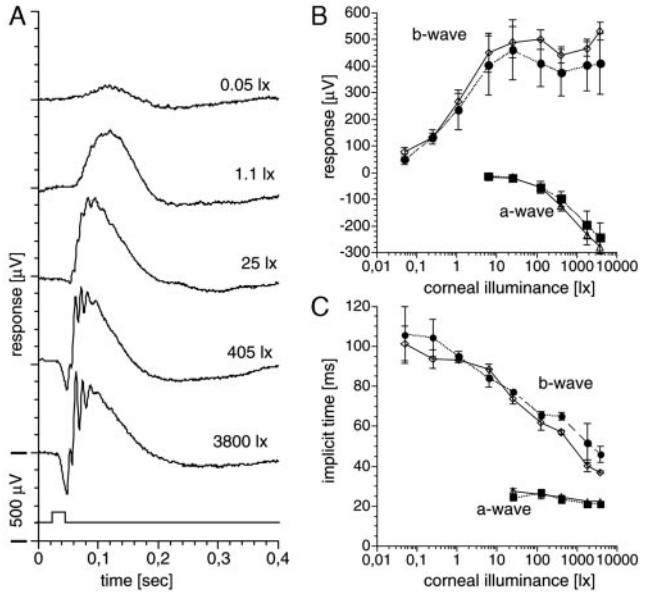

Figure 2. Scotopic ERG recordings. *A*, Example recordings of the dark-adapted ERG from a $Cx36^{-/-}$ $EGFP^{+}$ transgenic mouse in response to 20 msec white light flashes ranging from 0.05 to 3800 lux corneal illuminance. *B*, Intensity–response curves did not differ statistically for both the a-waves (squares, triangles) and b-waves (circles, diamonds) of $Cx36^{-/-}$ $EGFP^{+}$ (filled symbols) and $Cx36^{+/+}$ $EGFP^{-}$ mice (mean ± SEM; $n = 3$). *C*, Implicit time versus intensity of the a- and b-waves were also identical.

the region of the inner segments contain EGFP label. The scattered distribution of EGFP within the ONL and inner segments possibly reflects Cx36–EGFP being transported from the synthetic machinery in the cell body and inner segments to the axon terminals of photoreceptors. Electroretinogram (ERG) recordings of scotopic responses in this transgenic line revealed no differences from wild-type animals (data not shown). However, because endogenous Cx36 is still present in $Cx36^{Cx36-EGFP}$ mice, it is conceivable that functional gap junctions are composed of the original Cx36 and not of the EGFP-tagged variety. To investigate this possibility, we also performed ERG recordings on transgenic mice expressing the Cx36–EGFP fusion protein on a $Cx36^{-/-}$ background. As shown in Figure 2, there is no statistically significant difference from wild-type littermates, suggesting the presence of functional Cx36-containing gap junctions in the rod pathway of these transgenic mice (Fig. 2). Because endogenous Cx36 has been knocked out, function can only be restored by recruiting the EGFP-tagged transgene and targeting it to the appropriate subcellular locations.

In the second transgenic mouse line, $Cx36^{LacZ/LacZ}$, the Cx36 coding sequence located on exon 2 was replaced by a reporter gene encoding β-gal, and, in consequence, a fusion protein of the Cx36 N terminus, encoded by exon 1 and the β-gal protein (N36–β-gal), is expressed under the control of the Cx36 promoter. β-gal catalyzes the conversion of X-gal to a blue indolyl reaction product that appears confined to the endoplasmatic reticulum of Cx36-expressing cells. In the inner retina, cells in the ganglion cell layer and a single row of cells at the border between the inner nuclear layer (INL) and IPL are labeled (Fig. 1*D*). The latter cells correspond to AII amacrine cells, as described above. In the outer half of the INL, numerous small cell bodies are positive for X-gal. In addition, a few cells in the most distal part of the ONL express N36–β-gal. Both rod and cone photoreceptors are present in this outermost region of the mouse retina, whereas the inner half of the ONL exclusively contains rods. Thus, the staining pattern for N36–β-gal observed in the ONL indicates that Cx36 is present in cones rather than in rods.

Finally, strong labeling can be observed in the region of photoreceptor inner segments. The staining appears as X-gal-positive puncta alternating with regions that are devoid of any label (Fig. 1*D*). Because the endoplasmatic reticulum of photoreceptors is mainly localized in their inner segments, this discrete staining pattern most likely reflects expression of N36–β-gal in the inner segments of photoreceptors. In control experiments, wild-type mice never showed labeling of any of the retinal structures described above. Therefore, we consider expression of N36–β-gal as highly specific for Cx36-containing cells.

Expression of Cx36 in photoreceptors

Intracellular injections and immunocytochemistry

To determine the expression of Cx36 in photoreceptors, we injected individual rods and cones of $Cx36^{Cx36-EGFP}$ transgenic mice with the fluorescent dye Alexa 594. The confocal micrograph of Figure 3*A1* shows the typical morphology of a rod photoreceptor: outer and inner segments, and a small cell body with a long axon terminating in a lobular structure, the rod spherule. Superimposing a single 200-nm-thick optical section of the rod shown in Figure 3*A1* with the EGFP staining pattern demonstrates that Cx36 is not localized in the rod spherule (Fig. 3*A2*). Another rod spherule contacted by a rod bipolar cell is also negative for Cx36 (Fig. 3*C*). We performed this experiment for all optical sections of 10 different rods in three slice preparations and never observed localization of EGFP in rod spherules.

The same intracellular injection strategy was applied to label cones of $Cx36^{Cx36-EGFP}$ transgenic mice. As mentioned above, cell bodies of cones are almost exclusively found in the most distal region of the ONL, immediately adjacent to the outer limiting membrane. They can be rather easily identified for injection purposes because of their relatively large somata. The morphology of cones in the mouse retina is unmistakable, with a short outer segment, a large cell body, an axon, and an elaborate cone pedicle (Fig. 3*B1*). When superimposed on the corresponding EGFP section, cone pedicles almost always display colocalization (Fig. 3*B2*,*D*). We found EGFP in all cones injected ($n = 8$) but not in every single optical section, indicating restricted expression of Cx36 to some areas of the cone pedicle.

It is a general problem to unambiguously localize a dense punctate staining to homogeneously labeled cellular structures, because false positives caused by unspecific random colocalization cannot always be excluded. We therefore performed a statistical analysis on EGFP-positive puncta located on cone pedicles injected with fluorescent dyes. We found, on average, 10.25 ± 1.75 (mean ± SE; $n = 8$) EGFP-positive puncta per cone pedicle in a single optical section. However, when a mirror image of the EGFP staining pattern was projected onto the image of a corresponding cone, 4.87 ± 0.95 ($n = 8$) EGFP puncta per cone pedicle were obtained. When compared with the unswitched condition, these numbers are significantly different ($p < 0.05$; t test). Taking a different approach, the entire pedicle field of injected cones was tiled by 32 × 32 pixel squares. Every EGFP puncta located on a cone pedicle was centered on the brightest pixel. It has to be noted that, in their correct configuration, almost all EGFP puncta were found on the edge of the pedicle structure. When all of these squares ($n = 96$) were averaged, we obtained a distinct peak reflecting the localization of EGFP on the cone pedicle (Fig. 3*F*). Subsequently, we performed the same matrix calculations on the mirror image of the EGFP pattern projected onto the respective cones ($n = 98$). Under these conditions, colocal-

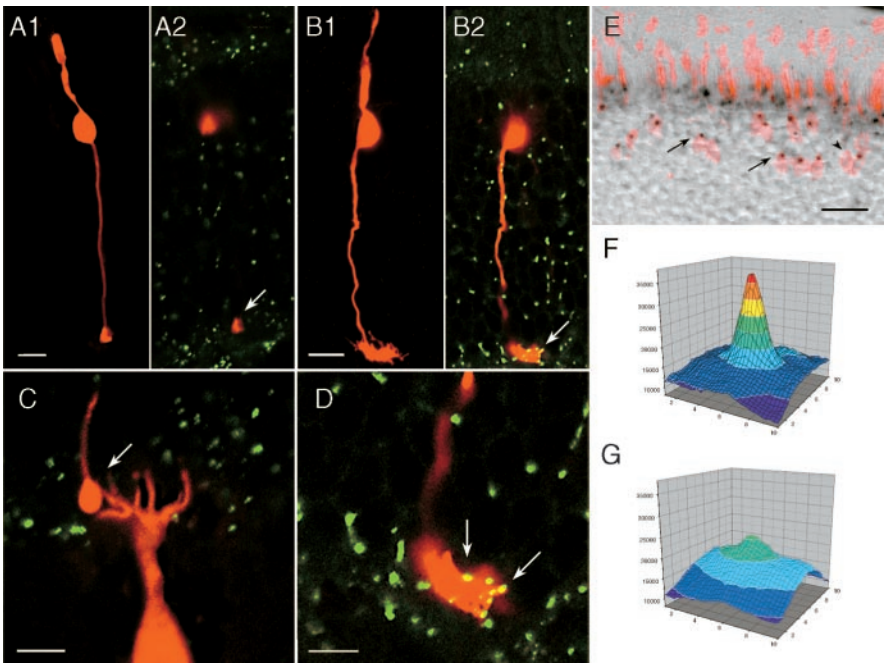

Figure 3. Expression of Cx36 in photoreceptors of $Cx36^{Cx36-EGFP}$ mice. *A1*, Stack of confocal images displaying the typical morphology of a rod photoreceptor injected with the fluorescent dye Alexa 594. *A2*, A 200 nm optical section of the rod shown in *A1* is superimposed with the EGFP staining pattern. EGFP is not localized in the rod spherule (arrow). *B1*, Stack of confocal images showing the typical morphology of a cone photoreceptor injected with the fluorescent dye Alexa 594. *B2*, A 200 nm optical section of the cone shown in *B1* is superimposed with the EGFP staining pattern. Cx36–EGFP appears to be expressed in the cone pedicle (arrow). *C*, Enlarged confocal micrograph of another rod spherule contacted by a rod bipolar cell. *D*, High-power confocal micrograph of the cone pedicle shown in *B* clearly reveals localization of EGFP-positive puncta at the cone pedicle (arrows). *E*, A vertical section of a $Cx36^{LacZ/LacZ}$ mouse retina counterstained with polyclonal antibodies directed against S-cone opsin. Both cell bodies (arrows) and inner segments of S-cones contain β-galactosidase-positive puncta. Very few S-cone somata do not express β-galactosidase (arrowhead). *F*, Localization of Cx36–EGFP on dye-injected cone pedicles results in a distinct peak in the center of the three-dimensional plot. *z*-axes numbers indicate brightness of the respective pixels. *G*, When a mirror image of the EGFP staining pattern is superimposed on the injected cones, colocalization of EGFP on cone pedicles is at chance levels, as indicated by the absence of a central peak. Scale bars: *A*, *C*, *D*, 5 μm; *B*, 10 μm; *E*, 20 μm.

ization of EGFP on cone pedicles appeared significantly reduced, as shown by the absence of a central peak (Fig. 3*G*). In those few cases in which colocalization occurred in the inverted configuration, EGFP puncta were almost always located in areas fully covered by the pedicle but not on the edge of the pedicle. In summary, the statistical analysis confirms that the colocalization of EGFP and dye-injected cones is not random but indicates expression of Cx36–EGFP in cone pedicles.

Finally, vertical sections of $Cx36^{LacZ/LacZ}$ mouse retina were counterstained with polyclonal antibodies directed against the S-cone opsin. As shown in Figure 3*E*, this antibody labels inner and outer segments as well as cell bodies of S-cones. With occasional exceptions, all somata positive for X-gal also display immunoreactivity against the S-cone opsin. Very rarely, however, S-cones do not contain X-gal reaction product (Fig. 3*E*, arrowhead). Because of the highly significant coincidence of β-gal-staining with S-cone opsin label in the region of the cell bodies as well as the inner segments, we conclude that Cx36 is expressed by S-cones in the mouse retina. Cx36 is most likely expressed by L/M-cones as well, as indicated by β-gal-positive cones that are not immunoreactive for S-cone opsin.

Reverse transcription-PCR

To obtain additional evidence for the differential expression of Cx36 in the ONL, samples of photoreceptors containing 20–30 cells each were harvested with a patch pipette in a vertical slice preparation. According to the distribution of rods and cones described above, cells were collected from the inner and outer half of the ONL, respectively (Fig. 4*A*). We applied reverse transcription PCR on these samples with two different sets of intron-spanning primers to detect mRNA of Cx36. The presence of rhodopsin mRNA served as a control for successful reverse transcription and to validate that our samples indeed contained photoreceptors (data not shown). In addition, we used whole retina samples to amplify a 447 bp product, which was specific for Cx36 transcript. Only those experiments with photoreceptor samples positive for rhodopsin and whole retina samples positive for Cx36 were considered for analysis.

Cells taken from the inner, rod-containing region of the ONL did not contain the message for Cx36 (24 samples) (Fig. 4*C*). However, we observed expression of Cx36 mRNA in 5 of 12 samples (42%) taken from the outer region of the ONL, which supposedly contains both rods and cones (Fig. 4*B*). The rather low number of positive outcomes is readily explained by the low cone-to-rod ratio in the mouse retina, deterioration of the already rare message, or inefficient amplification.

In summary, the data presented so far suggest that Cx36 is expressed in cone pedicles, thereby generating the diffuse staining pattern observed in the more scleral part of the OPL. In contrast to a recently published study (Deans et al., 2002), we found no evidence for expression of Cx36 in rod spherules.

Postsynaptic localization of Cx36

In addition to the punctate staining in cone pedicles, EGFP appears clustered in the lower, vitreal part of the OPL (Fig. 1*B*), suggesting expression of Cx36 in cells postsynaptic to photoreceptors. We performed double-labeling immunocytochemistry with antibodies to bassoon and synaptophysin as markers for presynaptic structures. In the OPL of the mammalian retina, bassoon immunoreactivity is found in ribbon synapses (Brandstätter et al., 1999), whereas antibodies against synaptophysin label photoreceptor terminals (Brandstätter et al., 1996). As expected, the staining patterns of bassoon and synaptophysin overlap significantly in a vertical section, thereby demarcating the presynaptic area of the OPL (Fig. 5*A*,*B*). However, patches of EGFP do not colocalize with the bassoon–synaptophysin label but rather appear as distinct entities below the photoreceptor terminals (Fig. 5*A*,*B*). These findings are confirmed by double labeling horizontal retinal sections of $Cx36^{Cx36-EGFP}$ mice against bassoon (Fig. 5*C*,*D*). Clusters of EGFP puncta appear in a different focal plane with respect to presynaptic markers, again indicating postsynaptic localization of Cx36. In horizontal sections, EGFP puncta form round or oval-shaped clusters containing, on average, 8.14 ± 2.53 (mean ± SD) discrete spots, with a diameter ranging from 0.27 to 0.57 μm (0.41 ± 0.08 μm) (Fig. 5*D*, inset). This value is in good accordance with ultrastructural data from Cx36-containing gap junctions between AII amacrine cells and ON-cone bipolar cells of the mouse retina (Tsukamoto et al., 2001).

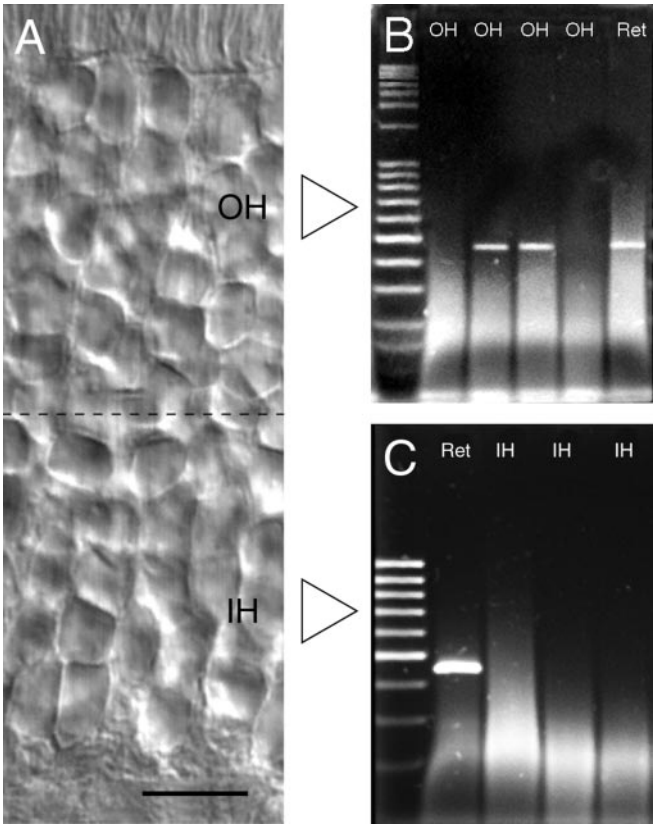

Figure 4. Agarose gel electrophoresis of reverse transcriptase PCR products for Cx36 mRNA. *A*, Micrograph of the ONL of wild-type mouse retina. The dotted line separates the inner, rod-containing half of the ONL (IH) and the outer half (OH), which is composed of both rods and cones. *B*, Cx36 mRNA was detected in samples taken from the outer half of the ONL. The molecular weight of the amplicon corresponds to the expected value (447 bp). *C*, Samples harvested from the inner half of the ONL were negative for Cx36 mRNA. Ret, Positive control performed with transcripts from whole mouse retina. Scale bar: *A*, 10 μm.

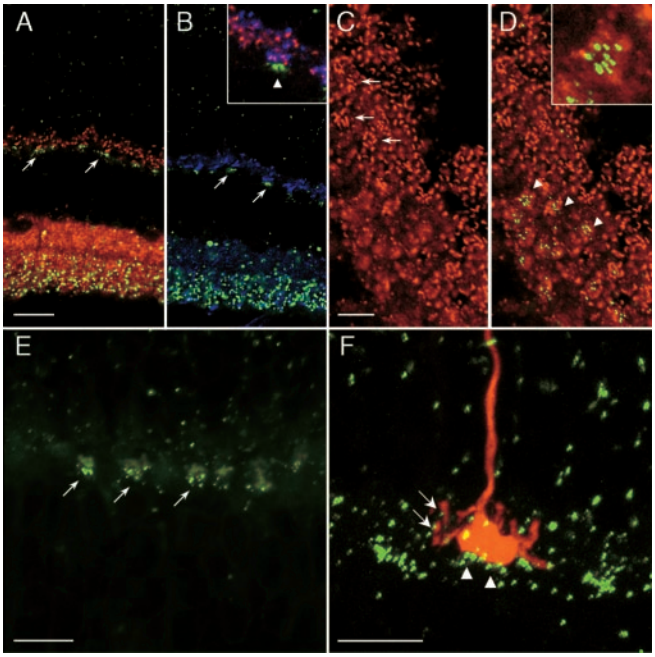

Figure 5. Expression of Cx36–EGFP patches in the OPL. *A*, *B*, Double labeling of Cx36–EGFP vertical section with antibodies against the presynaptic proteins bassoon (*A*) and synaptophysin (*B*). EGFP puncta appear as clusters that do not colocalize with presynaptic immunocytochemical markers (arrows). *B*, Inset, An enlarged confocal micrograph of a triple labeling, indicating postsynaptic location of Cx36–EGFP (arrowhead). *C*, Labeling of Cx36–EGFP horizontal sections with antibodies against bassoon. The section cuts the OPL in a slightly oblique way, with the INL in the bottom left and the ONL in the top right corner. Cone pedicles are easily identified according to the rosette-like arrangement of synaptic ribbons immunolabeled by bassoon (arrows). *D*, In the same section, EGFP clusters appear as round or oval accumulations of individual puncta, which do not colocalize with the bassoon-labeled cone pedicles, but are confined to a different focal plane (arrowheads). *D*, Inset, An enlarged confocal micrograph of EGFP-positive puncta on the diffuse background of an out-of-focus cone pedicle. *E*, Labeling of cone pedicles with PNA–FITC in a vertical section of $Cx36^{Cx36-EGFP}$ mouse retina. EGFP puncta appear clustered at the base of fluorescein-labeled cone pedicles (arrows). *F*, Dye-injected cone pedicle displays punctate (arrows) and clustered (arrowheads) Cx36–EGFP label on the presynaptic and postsynaptic side, respectively. Scale bars: *A*, *B*, 20 μm; *C–F*, 10 μm.

The number and distribution pattern of EGFP clusters in the OPL strongly suggest their spatial correlation with cone pedicles, albeit the clusters are not localized on the cone pedicles themselves. It has been shown that fluorescein isothiocyanate (FITC)-conjugated peanut agglutinin (PNA), a lectin with high affinity for galactose–galactosamine disaccharide residues, is specific for the synaptic region of cone photoreceptors (Blanks and Johnson, 1983). To demonstrate alignment of EGFP patches with cone pedicles, we labeled vertical sections of $Cx36^{Cx36-EGFP}$ mice with PNA–FITC. The diffuse cytoplasmic distribution of FITC is clearly distinct from the bright EGFP staining, which appears in perfect register with the population of PNA-labeled cone pedicles (Fig. 5*E*).

We obtained additional evidence by examining the alignment of EGFP and the pedicles of cones, which had been injected previously with the fluorescent dye Alexa 594 (Fig. 5*F*). In all cases ($n = 8$), we found accumulation of EGFP puncta at the base of the injected cone pedicles but obviously located on cells postsynaptic to the pedicle structure. In general, the spatial extent of EGFP clusters along the *z*-axes appeared considerably smaller than the footprint of the corresponding cone pedicle (Fig. 5*D*, inset).

Horizontal cells and rod bipolar cells

The staining pattern of EGFP described in the preceding section and the expression of N36–β-gal in the INL of $Cx36^{LacZ/LacZ}$ mice (Fig. 1*D*) indicate localization of Cx36 in cells postsynaptic to photoreceptors. Therefore, we examined whether Cx36 is expressed in horizontal cells, rod bipolar cells, or cone bipolar cells. Single-cell reverse transcriptase PCR combined with immunocytochemical detection of the intermediate filament protein vimentin indicate that Müller cells do not express Cx36 (data not shown).

The calcium-binding protein calbindin D28K is commonly used as a marker for horizontal cells in the rodent retina (Röhrenbeck et al., 1987). We showed previously that the retinal morphology of mice deficient for Cx36 is indistinguishable from wild-type animals in terms of cell types and cell numbers (Güldenagel et al., 2001). Therefore, we stained vertical sections of $Cx36^{LacZ/LacZ}$ mice for β-gal, followed by immunocytochemistry using polyclonal antibodies to calbindin. Calbindin-immunoreactive cell bodies in the outer INL are devoid of LacZ (Fig. 6*A*), indicating that horizontal cells do not contain Cx36.

Rod bipolar cells of the mammalian retina display protein kinase C (PKC)-like immunoreactivity (Greferath et al., 1990; Haverkamp and Wässle, 2000). Vertical sections of $Cx36^{Cx36-EGFP}$ mice were immunolabeled with monoclonal antibodies to the α-isoform of PKC. Figure 6*B* clearly shows that patches of EGFP appear exclusively in regions spared by rod bipolar cell dendrites (Fig. 3*C*). In addition, we found no evidence for expression of N36–β-gal

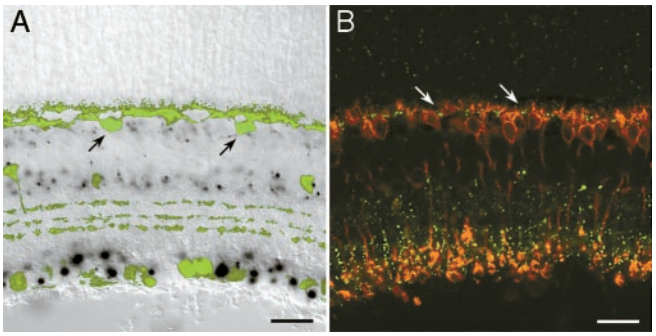

Figure 6. Cx36 is not expressed in horizontal cells and rod bipolar cells. *A*, Vertical section of a $Cx36^{LacZ/LacZ}$ mouse retina processed for β-galactosidase and calbindin-like immunocytochemistry. Cell bodies of horizontal cells do not contain β-gal reaction product (arrows). *B*, Confocal micrograph of PKC-like immunoreactivity in a vertical section of $Cx36^{Cx36-EGFP}$ mouse retina. Staining patterns of EGFP and PKC do not overlap (arrows), indicating that Cx36 is not expressed in rod bipolar cells. Scale bars, 20 μm.

in PKC-immunoreactive rod bipolar cell bodies (data not shown).

In summary, our findings indicate that Cx36 is not expressed in horizontal cells, rod bipolar cells, and Müller cells of the mouse retina, confirming two recently published studies (Deans and Paul, 2001; Deans et al., 2002).

OFF-cone bipolar cells

Next, we examined whether OFF-cone bipolar cells are the cellular source of clustered EGFP staining in the OPL. Bipolar cells with their axon terminals in the outermost part of the IPL are selectively labeled with antibodies directed against the neurokinin-3 receptor NK3R (Casini et al., 2000). In rat and mouse retina, NK3R labels at least two populations of OFF-cone bipolar cells (Haverkamp et al., 2003). In addition, the calcium-binding protein caldendrin can be used as a marker for OFF-cone bipolar cells in the mouse retina (Haverkamp and Wässle, 2000). Anti-NK3R and anti-caldendrin appear to label the same population of OFF-cone bipolar cells (Haverkamp et al., 2003). A third type of OFF-cone bipolar cell is selectively stained with antibodies against the hyperpolarization-activated cyclic nucleotide-gated potassium channel HCN4 (Müller et al., 2003).

Vertical sections of $Cx36^{Cx36-EGFP}$ mice were immunolabeled with polyclonal antibodies directed against NK3R and, in a separate experiment, caldendrin. Patches of EGFP puncta are located on the dendrites of NK3R-positive OFF-cone bipolar cells (Fig. 7*A*). We obtained the same result with sections of $Cx36^{Cx36-EGFP}$ mice stained against caldendrin (data not shown). Unfortunately, it was impossible to combine NK3R immunocytochemistry and X-gal histochemistry. Therefore, OFF-cone bipolar cells with an overall morphology similar to that of NK3R-positive cells were labeled by intracellular injections of $Cx36^{LacZ/LacZ}$ mice with the fluorescent dye Alexa 594 (Fig. 7*B*). The presence of the X-gal reaction product in the cell body confirms expression of Cx36 in type 1 and type 2 OFF-cone bipolar cells.

To investigate expression of Cx36 in other types, OFF-cone bipolar cells terminating in a slightly deeper stratum were injected in a vertical slice preparation of $Cx36^{Cx36-EGFP}$ mice. Superimposition of the EGFP staining pattern in 200 nm confocal sections indicates the presence of Cx36 in the dendrites of this type of OFF-cone bipolar cell (Fig. 7*C*). In addition, we performed immunocytochemistry against the potassium channel HCN4 in both $Cx36^{Cx36-EGFP}$ and $Cx36^{LacZ/LacZ}$ mice. This marker is present in type 3 OFF-cone bipolar cells, which terminate in a sublamina below the axon terminals of NK3R-positive OFF-cone bipolar cells. We routinely observed colocalization of Cx36–EGFP and HCN4 on the dendrites of bipolar cells (Fig. 7*D*), as well as expression of β-gal in HCN4-immunoreactive cell bodies (Fig. 7*E*). Both findings strongly suggest expression of Cx36 in type 3 OFF-cone bipolar cells. As described above, expression of Cx36 in all types of OFF-cone bipolar cell dendrites is spatially restricted to the area beneath the cone pedicle.

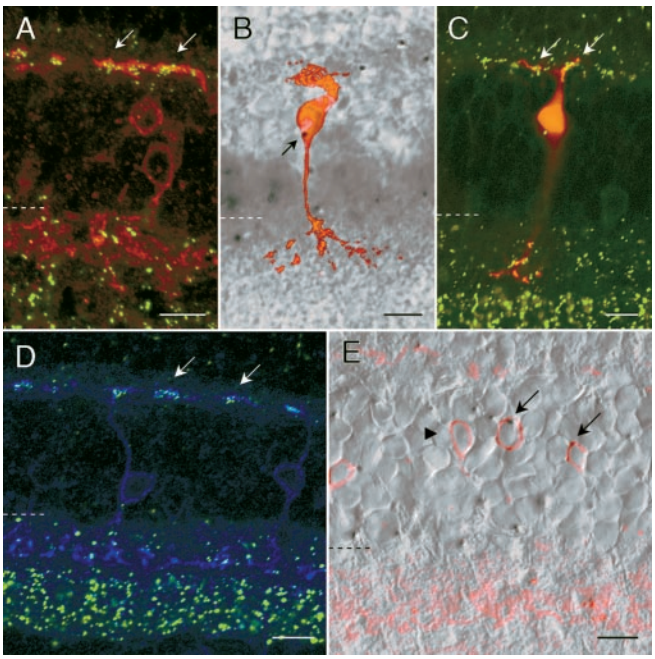

Figure 7. Expression of Cx36 in different types of OFF-cone bipolar cells. *A*, Vertical section of a $Cx36^{Cx36-EGFP}$ mouse retina immunolabeled with polyclonal antibodies to the neurokinin-3 receptor NK3R. Patches of EGFP colocalize with NK3R-positive dendrites of OFF-cone bipolar cells (arrows). *B*, Localization of β-galactosidase in a dye-injected OFF-cone bipolar cell (arrow). *C*, A 200 nm optical section obtained from a different type of OFF-cone bipolar cell demonstrates dendritic localization of EGFP puncta (arrows). *D*, Vertical section of a $Cx36^{Cx36-EGFP}$ mouse retina immunolabeled against the potassium channel HCN4. EGFP-positive puncta are localized to type 3 OFF-cone bipolar cell dendrites (arrows). *E*, Vertical section of a $Cx36^{LacZ/LacZ}$ mouse retina immunolabeled against HCN4 and superimposed on a transmission image. Most cell bodies of HCN4-positive OFF-bipolar cells express β-galactosidase (arrows), although few somata are devoid of the β-gal reaction product (arrowhead). Dotted lines indicate the INL–IPL border. Scale bars, 10 μm.

Expression of Cx36 and glutamate receptor subunits

Transmission of the light response from cones to OFF-cone bipolar cells is mediated by sign-conserving synapses using the amino acid glutamate. These synapses are located at non-invaginating or flat contacts characterized by the expression of ionotropic glutamate receptors at the postsynaptic side (Brandstätter et al., 1997; Haverkamp et al., 2000; Hack et al., 2001). In the mouse and rat retina, the AMPA receptor subunits GluR1 and GluR2 are predominantly found at flat contacts between cone pedicles and OFF-cone bipolar cells (Hack et al., 2001).

We labeled vertical sections from $Cx36^{Cx36-EGFP}$ mouse retina with antibodies against the AMPA receptor subunits GluR1, GluR2/3, and GluR4, against the kainate receptor subunit GluR5, and finally, with antibodies against the metabotropic glutamate receptor mGluR6. Interestingly, the staining patterns of EGFP and GluR1 showed significant colocalization, indicating close spatial vicinity of Cx36 and glutamate receptors containing the GluR1 subunit (Fig. 8*A*). We also found a spatial relationship

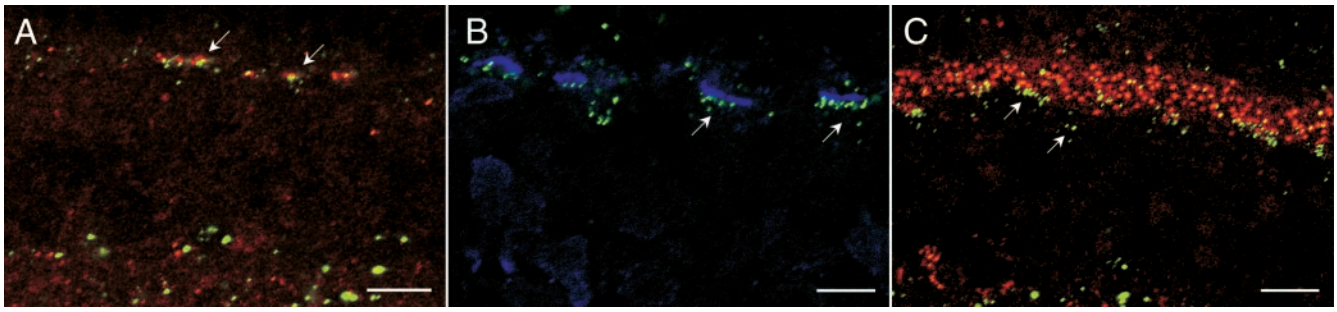

Figure 8. Spatial association of Cx36 with glutamate receptor subunits in the OPL. *A*, Confocal micrograph of a vertical section through $Cx36^{Cx36-EGFP}$ mouse retina labeled with polyclonal antibodies against GluR1. Arrows indicate close spatial relationship of Cx36–EGFP label and GluR1 immunoreactivity. *B*, Vertical section of a $Cx36^{Cx36-EGFP}$ mouse retina labeled with polyclonal antibodies against GluR5. Cx36–EGFP label appears associated with GluR5 but confined to a region below the GluR5 immunoreactivity (arrows). *C*, Vertical section of a $Cx36^{Cx36-EGFP}$ mouse retina labeled with polyclonal antibodies against the metabotropic glutamate receptor subtype mGluR6. mGluR6 is expressed on the dendrites of rod bipolar cells and ON-cone bipolar cells and is not associated with Cx36–EGFP (arrows). Scale bars, 10 μm.

between Cx36–EGFP and the kainate receptor subunit GluR5, which is also expressed by OFF-cone bipolar cells (Fig. 8*B*). However, it appears that Cx36–EGFP is located just beneath the GluR5 immunoreactivity. In contrast, we did not find a similar coincidence of Cx36 and glutamate receptors composed of GluR2/3 or GluR4 (data not shown). Finally, Cx36–EGFP and mGluR6, which is expressed in ON-cone bipolar cells and rod bipolar cells, do not colocalize beyond chance level (Fig. 8*C*).

Discussion

Transgenic mouse lines

We used two transgenic mouse lines to examine the expression of Cx36 in the outer mammalian retina (Fig. 9). The punctate staining pattern obtained by tagging Cx36 with EGFP reflects the distribution of Cx36-containing gap junctions in the retina, and therefore it is equivalent to immunolabeling with polyclonal antibodies specific for Cx36. In fact, we found a close-to-perfect match of EGFP and antibody distribution in the synaptic layers of the retina. Interestingly, C-terminal attachment of EGFP does not appear to prevent formation of functional gap junctions in the rod pathway.

In the second transgenic mouse line, the sequence coding for Cx36 on exon 2 was replaced by the histological reporter β-galactosidase, resulting in somatic labeling of N36–β-gal-expressing cells. Whereas the transgenic approach in $Cx36^{Cx36-EGFP}$ mice allows identification of the terminal location of Cx36, this second strategy reveals possible cell types expressing Cx36. Thus, the two transgenic lines provide complementary information on the expression pattern of Cx36. As shown previously, mice deficient in Cx36 have a normally developed retina and display no changes in the cellular organization of the rod pathway (Güldenagel et al., 2001).

Expression of Cx36 in cones

In our study, three lines of evidence indicate that Cx36 is expressed in cone photoreceptors: (1) targeting of Cx36–EGFP to cone pedicles, (2) colocalization of N36–β-gal and S-cone opsin in cell bodies of cones in the outermost ONL, and (3) detection of Cx36 mRNA in reverse transcriptase PCR samples obtained from the outer half of the ONL but not from the inner half. Deans et al. (2002), however, observed expression of β-gal throughout the ONL. Because rods constitute ~97% of all photoreceptors in the mouse retina (Jeon et al., 1998), the results obtained by Deans et al. (2002) suggest expression of Cx36 in rods. Currently, we have no explanation for this apparent discrepancy. However, it is possible that the simultaneous expression of two histological markers in a bicistronic construct as used by Deans et al. (2002) leads to a different labeling pattern.

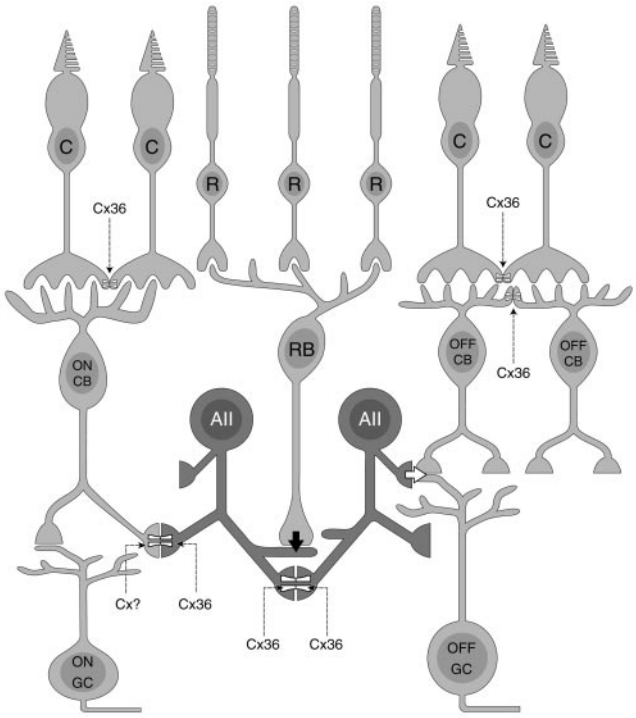

Figure 9. Schematic drawing indicating the distribution of Cx36 in the outer retina. Cone pedicles make homotypic gap junctions containing Cx36 with neighboring cone pedicles in the scleral part of the OPL. In addition, OFF-cone bipolar cells make homotypic, Cx36-containing gap junctions with other OFF-cone bipolar cells in the vitreal part of the OPL. These gap junctions appear restricted to an area outlined by the cone pedicle. Cx36-containing gap junctions in the rod pathway are also indicated. C, Cones; R, rods; CB, cone bipolar cells; RB, rod bipolar cells; AII, all amacrine cells; GC, ganglion cells.

It has to be noted that, in several of our specimens, the Cx36–EGFP staining pattern in the ONL appears too dense to be generated by cones only (Fig. 3*B2*). The same holds true for the number of LacZ-positive puncta in the region of the inner segments (Fig. 1*D*), which do not always colocalize with the S-cone opsin staining. It is conceivable that those inner segments that contain β-gal but are negative for S-cone opsin correspond to L/M-cones. However, given the high density of EGFP-positive puncta in the ONL and expression of β-gal in the inner segments,

we cannot finally exclude expression of Cx36 in rods. To answer this question, the entire population of cones in the mouse retina has to be labeled, and its staining pattern matched to the distribution of both EGFP and LacZ.

Multiple rod pathways have been hypothesized in the mammalian retina. In the primary pathway, rods connect to rod bipolar cells, which relay their signal to AII amacrine cells. These cells serve as an interface for transmitting the rod signal into the cone pathway, by both glycinergic synapses and electrical synapses involving Cx36 (Feigenspan et al., 2001; Mills et al., 2001). Cx36-containing gap junctions between AII amacrine cells and ON-cone bipolar cells are essential for normal synaptic transmission in the primary rod pathway (Güldenagel et al., 2001). A second rod pathway was suggested based on the presence of gap junctions between rods and cones (Raviola and Gilula, 1973; Smith et al., 1986). It is assumed that rod–cone coupling provides the structural basis for the rod signal to enter ON-cone and OFF-cone bipolar cells. Extracellular recordings of ON-ganglion cells performed in Cx36 knock-out animals reveal complete elimination of rod-mediated responses (Deans et al., 2002). Because intermediate-sensitivity responses also disappear, this finding was interpreted as evidence for involvement of Cx36 in both of the rod pathways outlined above. Alternatively, if two signals were generated within the same rod, as shown for primate rod photoreceptors (Schneeweis and Schnapf, 1995), Cx36 would not be required in gap junctions between rods and cones.

In other mammalian species, Cx36 appears to be involved in both cone–cone and rod–cone coupling, although it seems to be expressed exclusively by cones (Lee et al., 2003). Our results reveal that Cx36–EGFP puncta are not located close enough to rod spherules to contribute to rod–cone coupling in the mouse retina. In the mammalian retina, especially the primate fovea, small gap junctions between cone pedicles have been demonstrated (Raviola and Gilula, 1973; Tsukamoto et al., 2001). Adjacent cones are in close physical contact (Zhu et al., 2002), which is a prerequisite for cone–cone coupling. Paired recordings of cones performed in the ground squirrel retina have indeed demonstrated that cone–cone coupling improves the signal-to-noise ratio without compromising visual acuity (DeVries et al., 2002). Therefore, cone–cone coupling in the mouse retina is likely to play a similar physiological role.

Expression of Cx36 in OFF-cone bipolar cells

In $Cx36^{Cx36-EGFP}$ mouse retina, EGFP label accumulates on dendrites of OFF-cone bipolar cells. These patches of EGFP are confined to an area just below the base of the cone pedicle, and there is always only one patch per pedicle. OFF-bipolar cells expressing Cx36 are immunoreactive for NK3R, caldendrin, and HCN4, thus comprising at least three different cell types.

At present, we can only speculate on the physiological significance of Cx36-containing gap junctions on dendrites of OFF-cone bipolar cells. In the mouse retina, cone pedicles contain, on average, 10 ribbon synapses (Tsukamoto et al., 2001), suggesting transmission of the cone signal to a similar number of postsynaptic bipolar cells. A cluster of EGFP signals underlying the cone pedicle is composed of eight Cx36-containing gap junctions on average, indicating that at least some OFF-cone bipolar cells contacting a single cone pedicle are electrically coupled. Because Cx36-expressing bipolar cells belong to the OFF variety, their membrane potential is rather depolarized in the dark and hyperpolarized in the light. The depolarizing signal, induced by the release of glutamate from a single cone pedicle and the subsequent binding of transmitter to ionotropic glutamate receptors on the postsynaptic membrane, is likely to affect all connected bipolar cells of a given type differently. Consequently, the efficacy of signal transmission onto ganglion cells will vary according to the membrane potential of glutamate-releasing bipolar cells. Therefore, providing bipolar cell dendrites with a low-resistance electrical pathway could equilibrate the membrane potential within the network of coupled cells, eventually decreasing blur of the cone signal. This would be especially effective if the dynamics of coupling were linked to transmitter release at the cone-to-bipolar cell synapse.

Colocalization of Cx36–EGFP and glutamate receptor subunits

In a recent study, the AMPA receptor subunits GluR1 and GluR2 were predominantly found at flat contacts established between cone pedicles and OFF-cone bipolar cells (Hack et al., 2001). On the level of the light microscope, Cx36–EGFP and GluR1 appear in close spatial proximity, whereas there is no such relationship with other AMPA receptor subunits. The kainate receptor subunit GluR5 does not colocalize with GluR1 on the dendrites of OFF-cone bipolar cells (Haverkamp et al., 2001). Similarly, we did not observe colocalization of Cx36 and GluR5.

The close proximity of Cx36 and GluR1 suggests a role of glutamate receptors containing this subunit in the regulation of gap junctions. Modulation of gap junction coupling of astroglia and cerebellar Bergmann glial cells by glutamate receptor activation has been described previously (Enkvist and McCarthy, 1994; Müller et al., 1996). This effect is most likely caused by the increased influx of calcium through ionotropic glutamate receptor channels. Recently, the fish homolog of Cx36, Cx35, has been shown to mediate electrical transmission at Mauthner cell mixed synapses (Pereda et al., 2003). It is conceivable that activity-driven interactions between chemical and electrical synapses are not limited to mixed synapses but will occur when chemical synapses are located sufficiently close to gap junction plaques (Pereda et al., 1998; Smith and Pereda, 2003). Therefore, influx of calcium through GluR1-containing AMPA receptors could regulate gap junction permeability of OFF-cone bipolar cells and thus provide a link between synaptic activity and synchronization of a postsynaptic network of coupled cells.

We did not observe any spatial relationship between Cx36–EGFP and mGluR6. Because rod bipolar cells outnumber ON-cone bipolar cells in the mouse retina, we do not consider this immunocytochemical result as sufficient evidence to exclude expression of Cx36 in ON-cone bipolar cells. However, on the basis of their respective expression patterns, a functional interaction between Cx36 and mGluR6 seems very unlikely.

In conclusion, glutamate released from cone pedicles at flat contacts is likely to have a twofold effect on its postsynaptic targets. Binding to ionotropic glutamate receptors induces depolarization of OFF-cone bipolar cells, i.e., the classical sign-conserving transmission of visual information in the OFF pathway. Simultaneously, the influx of calcium ions through the very same glutamate receptor channels influences gap junction permeability between interconnected OFF-cone bipolar cells, eventually leading to averaging of voltage changes within a population of OFF-cone bipolar cells.

References

Benardo LS (1997) Recruitment of GABAergic inhibition and synchronization of inhibitory interneurons in rat neocortex. J Neurophysiol 77:3134–3144.

Blanks JC, Johnson LV (1983) Selective lectin binding of the developing mouse retina. J Comp Neurol 221:31–41.

Brandstätter JH, Löhrke S, Morgans CW, Wässle H (1996) Distributions of two homologous synaptic vesicle proteins, synaptoporin and synaptophysin, in the mammalian retina. J Comp Neurol 370:1–10.

Brandstätter JH, Koulen P, Wässle H (1997) Selective synaptic distribution of kainate receptor subunits in the two plexiform layers of the rat retina. J Neurosci 17:9298–9307.

Brandstätter JH, Fletcher EL, Garner CC, Gundelfinger ED, Wässle H (1999) Differential expression of the presynaptic cytomatrix protein bassoon among ribbon synapses in the mammalian retina. Eur J Neurosci 11:3683–3693.

Casini G, Brecha NC, Bosco L, Rickman DW (2000) Developmental expression of neurokinin-1 and neurokinin-3 receptors in the rat retina. J Comp Neurol 421:275–287.

Condorelli DF, Belluardo N, Trovato-Salinaro A, Mudo G (2000) Expression of Cx36 in mammalian neurons. Brain Res Brain Res Rev 32:72–85.

De Zeeuw CI, Chorev E, Devor A, Manor Y, Van Der Giessen RS, De Jeu MT, Hoogenraad CC, Bijman J, Ruigrok TJ, French P, Jaarsma D, Kistler WM, Meier C, Petrasch-Parwez E, Dermietzel R, Söhl G, Güldenagel M, Willecke K, Yarom Y (2003) Deformation of network connectivity in the inferior olive of connexin 36-deficient mice is compensated by morphological and electrophysiological changes at the single neuron level. J Neurosci 23:4700–4711.

Deans MR, Paul DL (2001) Mouse horizontal cells do not express connexin26 or connexin36. Cell Commun Adhes 8:361–366.

Deans MR, Gibson JR, Sellitto C, Connors BW, Paul DL (2001) Synchronous activity of inhibitory networks in neocortex requires electrical synapses containing connexin36. Neuron 31:477–485.

Deans MR, Volgyi B, Goodenough DA, Bloomfield SA, Paul DL (2002) Connexin36 is essential for transmission of rod-mediated visual signals in the mammalian retina. Neuron 36:703–712.

DeVries SH, Qi X, Smith R, Makous W, Sterling P (2002) Electrical coupling between mammalian cones. Curr Biol 12:1900–1907.

Draguhn A, Traub RD, Schmitz D, Jefferys JG (1998) Electrical coupling underlies high-frequency oscillations in the hippocampus in vitro. Nature 394:189–192.

Eiberger J, Degen J, Romualdi A, Deutsch U, Willecke K, Söhl G (2001) Connexin genes in the mouse and human genome. Cell Commun Adhes 8:163–165.

Enkvist MO, McCarthy KD (1994) Astroglial gap junction communication is increased by treatment with either glutamate or high K^+ concentration. J Neurochem 62:489–495.

Feigenspan A, Teubner B, Willecke K, Weiler R (2001) Expression of neuronal connexin36 in AII amacrine cells of the mammalian retina. J Neurosci 21:230–239.

Galarreta M, Hestrin S (1999) A network of fast-spiking cells in the neocortex connected by electrical synapses. Nature 402:72–75.

Gibson JR, Beierlein M, Connors BW (1999) Two networks of electrically coupled inhibitory neurons in neocortex. Nature 402:75–79.

Greferath U, Grünert U, Wässle H (1990) Rod bipolar cells in the mammalian retina show protein kinase C-like immunoreactivity. J Comp Neurol 301:433–442.

Güldenagel M, Söhl G, Plum A, Traub O, Teubner B, Weiler R, Willecke K (2000) Expression patterns of connexin genes in mouse retina. J Comp Neurol 425:193–201.

Güldenagel M, Ammermüller J, Feigenspan A, Teubner B, Degen J, Söhl G, Willecke K, Weiler R (2001) Visual transmission deficits in mice with targeted disruption of the gap junction gene connexin36. J Neurosci 21:6036–6044.

Hack I, Frech M, Dick O, Peichl L, Brandstätter JH (2001) Heterogeneous distribution of AMPA glutamate receptor subunits at the photoreceptor synapses of rodent retina. Eur J Neurosci 13:15–24.

Haverkamp S, Wässle H (2000) Immunocytochemical analysis of the mouse retina. J Comp Neurol 424:1–23.

Haverkamp S, Grünert U, Wässle H (2000) The cone pedicle, a complex synapse in the retina. Neuron 27:85–95.

Haverkamp S, Grünert U, Wässle H (2001) Localization of kainate receptors at the cone pedicles of the primate retina. J Comp Neurol 436:471–486.

Haverkamp S, Ghosh KK, Hirano AA, Wässle H (2003) Immunocytochemical description of five bipolar cell types of the mouse retina. J Comp Neurol 455:463–476.

Hormuzdi SG, Pais I, LeBeau FE, Towers SK, Rozov A, Buhl EH, Whittington MA, Monyer H (2001) Impaired electrical signaling disrupts gamma frequency oscillations in connexin 36-deficient mice. Neuron 31:487–495.

Jeon CJ, Strettoi E, Masland RH (1998) The major cell populations of the mouse retina. J Neurosci 18:8936–8946.

Lee EJ, Han JW, Kim HJ, Kim IB, Lee MY, Oh SJ, Chung JW, Chun MH (2003) The immunocytochemical localization of connexin 36 at rod and cone gap junctions in the guinea pig retina. Eur J Neurosci 18:2925–2934.

Mann-Metzer P, Yarom Y (1999) Electrotonic coupling interacts with intrinsic properties to generate synchronized activity in cerebellar networks of inhibitory interneurons. J Neurosci 19:3298–3306.

Meier C, Petrasch-Parwez E, Habbes HW, Teubner B, Güldenagel M, Degen J, Söhl G, Willecke K, Dermietzel R (2002) Immunohistochemical detection of the neuronal connexin36 in the mouse central nervous system in comparison to connexin36-deficient tissues. Histochem Cell Biol 117:461–471.

Mills SL, O'Brien JJ, Li W, O'Brien J, Massey SC (2001) Rod pathways in the mammalian retina use connexin 36. J Comp Neurol 436:336–350.

Müller F, Scholten A, Ivanova E, Haverkamp S, Kremmer E, Kaupp UB (2003) HCN channels are expressed differentially in retinal bipolar cells and concentrated at synaptic terminals. Eur J Neurosci 17:2084–2096.

Müller T, Moller T, Neuhaus J, Kettenmann H (1996) Electrical coupling among Bergmann glial cells and its modulation by glutamate receptor activation. Glia 17:274–284.

Pereda A, O'Brien J, Nagy JI, Bukauskas F, Davidson KG, Kamasawa N, Yasumura T, Rash JE (2003) Connexin35 mediates electrical transmission at mixed synapses on Mauthner cells. J Neurosci 23:7489–7503.

Pereda AE, Bell TD, Chang BH, Czernik AJ, Nairn AC, Soderling TR, Faber DS (1998) Ca^{2+}/calmodulin-dependent kinase II mediates simultaneous enhancement of gap-junctional conductance and glutamatergic transmission. Proc Natl Acad Sci USA 95:13272–13277.

Rash JE, Staines WA, Yasumura T, Patel D, Furman CS, Stelmack GL, Nagy JI (2000) Immunogold evidence that neuronal gap junctions in adult rat brain and spinal cord contain connexin-36 but not connexin-32 or connexin-43. Proc Natl Acad Sci USA 97:7573–7578.

Raviola E, Gilula NB (1973) Gap junctions between photoreceptor cells in the vertebrate retina. Proc Natl Acad Sci USA 70:1677–1681.

Röhrenbeck J, Wässle H, Heizmann CW (1987) Immunocytochemical labelling of horizontal cells in mammalian retina using antibodies against calcium-binding proteins. Neurosci Lett 77:255–260.

Schneeweis DM, Schnapf JL (1995) Photovoltage of rods and cones in the macaque retina. Science 268:1053–1056.

Smith M, Pereda AE (2003) Chemical synaptic activity modulates nearby electrical synapses. Proc Natl Acad Sci USA 100:4849–4854.

Smith RG, Freed MA, Sterling P (1986) Microcircuitry of the dark-adapted cat retina: functional architecture of the rod-cone network. J Neurosci 6:3505–3517.

Strata F, Atzori M, Molnar M, Ugolini G, Tempia F, Cherubini E (1997) A pacemaker current in dye-coupled hilar interneurons contributes to the generation of giant GABAergic potentials in developing hippocampus. J Neurosci 17:1435–1446.

Tamas G, Buhl EH, Lorincz A, Somogyi P (2000) Proximally targeted GABAergic synapses and gap junctions synchronize cortical interneurons. Nat Neurosci 3:366–371.

Theis M, de Wit C, Schlaeger TM, Eckardt D, Krüger O, Döring B, Risau W, Deutsch U, Pohl U, Willecke K (2001) Endothelium-specific replacement of the connexin43 coding region by a lacZ reporter gene. Genesis 29:1–13.

Traub RD, Schmitz D, Jefferys JG, Draguhn A (1999) High-frequency population oscillations are predicted to occur in hippocampal pyramidal neuronal networks interconnected by axoaxonal gap junctions. Neuroscience 92:407–426.

Tsukamoto Y, Morigiwa K, Ueda M, Sterling P (2001) Microcircuits for night vision in mouse retina. J Neurosci 21:8616–8623.

Venance L, Rozov A, Blatow M, Burnashev N, Feldmeyer D, Monyer H (2000) Connexin expression in electrically coupled postnatal rat brain neurons. Proc Natl Acad Sci USA 97:10260–10265.

Willecke K, Eiberger J, Degen J, Eckardt D, Romualdi A, Güldenagel M, Deutsch U, Söhl G (2002) Structural and functional diversity of connexin genes in the mouse and human genome. Biol Chem 383:725–737.

Zhu X, Li A, Brown B, Weiss ER, Osawa S, Craft CM (2002) Mouse cone arrestin expression pattern: light induced translocation in cone photoreceptors. Mol Vis 8:462–471.